

CUTS+: High-dimensional Causal Discovery from Irregular Time-series

Yuxiao Cheng^{1*} Lianglong Li^{1*} Tingxiong Xiao¹ Zongren Li³ Qin Zhong³
Jinli Suo^{12†} Kunlun He^{3†}

¹Department of Automation, Tsinghua University

²Institute for Brain and Cognitive Science, Tsinghua University (THUIBCS)

³Chinese PLA General Hospital

Abstract

Causal discovery in time-series is a fundamental problem in the machine learning community, enabling causal reasoning and decision-making in complex scenarios. Recently, researchers successfully discover causality by combining neural networks with Granger causality, but their performances degrade largely when encountering high-dimensional data because of the highly redundant network design and huge causal graphs. Moreover, the missing entries in the observations further hamper the causal structural learning. To overcome these limitations, we propose CUTS+, which is built on the Granger-causality-based causal discovery method CUTS and raises the scalability by introducing a technique called coarse-to-fine-discovery (C2FD) and leveraging a message-passing-based graph neural network (MPGNN). Compared to previous methods on simulated, quasi-real, and real datasets, we show that CUTS+ largely improves the causal discovery performance on high-dimensional data with different types of irregular sampling.

Introduction

Analyzing complex interactions behind the observed time-series, i.e., time-series analysis, is a fundamental problem in machine learning and holds great potential in various real-world applications. However, revealing the complex relationships buried under massive amounts of variables can be challenging for algorithm design. Recently, approaches have been proposed to extract causal relationships from observational data (Tank et al. 2022; Löwe et al. 2022; Khanna and Tan 2020; Runge et al. 2019; Cheng et al. 2023; Xu, Huang, and Yoo 2019). This task is called time-series causal discovery, which serves as a fundamental tool in machine learning by enabling causal reasoning of time-series.

Although proven to be able to efficiently discover causal relationships, most of these methods lack the ability to handle high-dimensional time-series. Actually, many causal discovery algorithms are only tested on datasets with fewer than 20 time-series (i.e. $N \leq 20$) (Tank et al. 2022; Khanna and Tan 2020), while the real time-series datasets often contain dozens or even hundreds of time-series, e.g., gene regulation networks or air quality index. Recently, Cheng et al. (2023) proposed CUTS, an iterative approach to jointly perform causal graph learning and missing data imputation

for irregular temporal data. Although CUTS is proposed to boost causal discovery with data imputation and the other way around, the data prediction module is composed of component-wise LSTMs and MLPs with redundant structures and parameters, hampering the scalability when encountering high-dimensional datasets. Moreover, the causal graph in CUTS can be too large to learn with high accuracy.

To overcome these issues, we propose **CUTS+**, an extension of CUTS with scalability to high-dimensional time-series, via proposing two specially designed techniques: coarse-to-fine causal discovery (C2FD) and message-passing graph neural network (MPGNN) for data prediction. Our contributions include:

- We propose CUTS+, upgrading CUTS (Cheng et al. 2023) to largely increase the scalability towards high-dimensional time-series. Specifically, we leverage two novel techniques, i.e., Coarse-to-fine-discovery (C2FD), a simple yet efficient technique to facilitate scalable causal graph optimization, and message-passing-based graph neural network (MPGNN) to remove structural redundancy in CUTS+.
- With extensive experiments, we show that CUTS+ largely increases causal discovery performance and decreases time cost, especially on high-dimensional datasets, with either multiple types of irregular sampling or no missing values.

Related Works

Causal Structural Learning / Causal Discovery. Existing Causal Structural Learning (or Causal Discovery) approaches can be categorized into five classes. (i) *Constraint-based approaches*, such as PC (Spirtes and Glymour 1991), FCI (Spirtes et al. 2000), and PCMCI (Runge et al. 2019; Runge 2020; Gerhardus and Runge 2020), build causal graphs by conditional independence tests. (ii) *Score-based learning algorithms* which include penalized Neural Ordinary Differential Equations and acyclicity constraint (Bellot, Branson, and van der Schaar 2022) (Pamfil et al. 2020). (iii) *Convergent Cross Mapping (CCM)* proposed by Sugihara et al. (2012) that reconstructs nonlinear state space for nonseparable weakly connected dynamic systems. This approach is later extended to situations of synchrony, confounding, or sporadic time series (Ye et al. 2015; Benkő

*Equal Contribution

et al. 2020; Brouwer et al. 2021). (iv) Approaches based on *Additive Noise Model (ANM)* that infer causal graph based on additive noise assumption (Shimizu et al. 2006; Hoyer et al. 2008). ANM is extended by Hoyer et al. (2008) to nonlinear models with almost any nonlinearities. (v) *Granger-causality-based* approaches. Granger causality is initially introduced by Granger (1969) who proposed to analyze the temporal causal relationships by testing the help of a time-series on predicting another time-series. Recently, Deep Neural Networks (NNs) are widely applied to infer nonlinear Granger causality since the central idea of Granger Causality is highly compatible with NNs. Researchers have successfully use Recurrent Neural Networks (RNNs) or other NNs for time series analysis to discover causal graphs (Wu, Singh, and Berger 2022; Tank et al. 2022; Khanna and Tan 2020; Löwe et al. 2022; Cheng et al. 2023). This work also incorporates a deep neural network to discover Granger Causality.

Scalable / High-dimensional Causal Discovery. Scalability can be a serious problem when applying causal discovery algorithms to real data. With hundreds of time-series (or hundreds of static nodes), the potential possibility for causal relations grows exponentially. Existing approaches may fail because they involve either massive conditional independence tests (Runge et al. 2019), too many variables to be conditioned on (Hong, Liu, and Mai 2017), or large quantities of parameters to be optimized (Tank et al. 2022; Cheng et al. 2023). To solve this problem, scalable or high-dimensional causal discovery approaches are proposed. In static settings, Hong, Liu, and Mai (2017) and Morales-Alvarez et al. (2022) propose to boost scalability via divide-and-conquer technique, Lopez et al. (2022) limit the search space to low-rank factor graphs, Cundy, Grover, and Ermon (2021) instead leverages variational framework. In time-series settings like ours, the scalability issue is less explored. The most related work to ours is Xu, Huang, and Yoo (2019)’s which also uses Granger causality and simplifies the high-dimensional adjacency matrix with low-rank approximation. However, the low-rank assumption may not be satisfied in real scenarios. Our CUTS+ is an extension of Granger-causality-based approaches by alleviating the scalability issue without low-rank approximation.

Background

Time Series and Granger Causality

We inherit the notation in (Cheng et al. 2023) and denote a uniformly sampled observation of a dynamic system as $\mathbf{X} = \{\mathbf{x}_{i,1:T}\}_{i=1}^N$, where $x_{i,t}$ represents the i th time-series sampled at time point t , and $t \in \{1, \dots, T\}$, $i \in \{1, \dots, N\}$, with T and N being the length and number of the time-series. Each sampled variable $x_{i,t}$ is assumed to be generated by the following Structural Causal Model (SCM) with additive noise:

$$x_{i,t} = f_i(\mathbf{x}_{1,t-\tau:t-1}, \mathbf{x}_{2,t-\tau:t-1}, \dots, \mathbf{x}_{N,t-\tau:t-1}) + e_{i,t} \quad (1)$$

in which τ denotes the maximal time lag and $i = 1, 2, \dots, N$. Our CUTS+ can also handle irregular time-series by jointly performing imputation and causal discovery. So to model the

irregular time-series, a bi-value observation mask $o_{t,i}$ is used to label the missing entries, i.e., the observed point equals the generated $x_{i,t}$ when $o_{t,i}$ equals to 1. In this paper, we adopt the protocols of previous works (Yi et al. 2016; Cini, Marisca, and Alippi 2022) and consider two types of data missing that often occur in practical observations:

- *Random Missing (RM)*. The data entries in the observations are missing with a certain probability p , here in our experiments the missing probability follows Bernoulli distribution $o_{t,i} \sim \text{Ber}(1 - p)$.
- *Random Block Missing (RBM)*. Under a relatively small p for RM, we set a block failure probability p_{blk} and block length $L_{\text{blk}} \sim \text{Uniform}(L_{\text{min}}, L_{\text{max}})$, i.e. there exist $p_{\text{blk}} \cdot N \cdot T$ missing blocks on average and each with length uniformly distributed in $[L_{\text{min}}, L_{\text{max}}]$.

Note that these two types can both be categorized into Missing Complete at Random (MCAR), a most common type of data missing (Geffner et al. 2022). In this work, we build on the Granger causality. Actually, Granger causality is not necessarily SCM-based causality, since the latter one often considers acyclicity. Under the assumptions of no unobserved variables and no instantaneous effects, Peters, Janzing, and Schölkopf (2017) shows identifiability of time-invariant Granger causality (Löwe et al. 2022; Vowels, Camgoz, and Bowden 2021). For a dynamic system, time-series i Granger causes time-series j when the past values of time-series \mathbf{x}_i aid in the prediction of the current and future status of time-series \mathbf{x}_j . Specifically, we adapt the definition from (Tank et al. 2022) that time-series i is Granger non-causal of j if there exists $\mathbf{x}'_{i,t-\tau:t-1} \neq \mathbf{x}_{i,t-\tau:t-1}$ satisfying

$$\begin{aligned} f_j(\mathbf{x}_{1,t-\tau:t-1}, \dots, \mathbf{x}'_{i,t-\tau:t-1}, \dots, \mathbf{x}_{N,t-\tau:t-1}) &= \\ f_j(\mathbf{x}_{1,t-\tau:t-1}, \dots, \mathbf{x}_{i,t-\tau:t-1}, \dots, \mathbf{x}_{N,t-\tau:t-1}) & \end{aligned} \quad (2)$$

i.e., the past data points of time-series i influence the prediction of $x_{j,t}$. For simplicity, we use \mathbf{x}_i to denote $\mathbf{x}_{i,t-\tau:t-1}$ in the following. The discovered pair-wise Granger causal relationship is a directed graph, which is then represented with an adjacency matrix $\mathbf{A} = \{a_{ij}\}_{i,j=1}^N$, where $a_{ij} = 1$ denotes time-series i Granger causes j and $a_{ij} = 0$ means otherwise. The idea of Granger causality is highly compatible with the basic idea of neural networks (NNs) since NNs can serve as powerful predictors. In previous works, (Cheng et al. 2023) prove that causal graph discovery in their CUTS converges to the true graphs under the Additive Noise Model and Universal Approximation Theorem, which again validates the successful combination of Granger causality and NNs.

Difficulties with High Dimensional Time-series

In real scenarios, it is common to face hundreds of long time-series with complex causal graphs. We now proceed to show difficulties when CUTS or other causal discovery algorithms handle such data.

Large Adjacency Matrix. The pairwise GC relationship, denoted as matrix $\mathbf{A}_{N \times N}$, can become very large as N increases. Prior works mainly focus on the settings when $N \leq 20$ (Tank et al. 2022; Khanna and Tan 2020; Cheng et al. 2023), and we show in the experiments that their performances degrade greatly when $N > 20$. Alternatively, Xu,

CPG	Causal Probability Graph M
GCPG	Group CPG Q
BCG	Binary Causal Graph S
MPNN	Message-Passing NN
MPGNN	Message-Passing GNN
C2FD	Coarse-to-fine Causal Discovery

Table 1: List of abbreviations.

Huang, and Yoo (2019) addresses the scalability issue at increasing data dimension via conducting low-rank approximation to the adjacency matrix, but the strong low-rank assumption of $\mathbf{A}_{N \times N}$ does not hold in many scenarios.

Redundancy of cMLP / cLSTM. To uncover the black-box of NNs, Cheng et al. (2023); Tank et al. (2022) disentangle causal effects from causal parents to individual output series. As a result, one must use N separate MLPs / LSTMs to ensure the disentanglement. This is called component-wise MLP / LSTM (cMLP / cLSTM) and frequently used when discovering Granger causality (Khanna and Tan 2020). In the following We formalize component-wise neural networks as ‘‘causally disentangled neural networks’’.

Definition 1 Let $\mathbf{x} \in \mathcal{X} \subset \mathbb{R}^n$, $\mathbf{A} \in \mathcal{A} \subset \{0, 1\}^{n \times n}$ and $\mathcal{Y} \subset \mathbb{R}^n$ be the input and output spaces. We say a neural network $\mathbf{f}_\Theta : (\mathcal{X}, \mathcal{A}) \rightarrow \mathcal{Y}$ is a **causally disentangled neural network (CDNN)** if it has the form

$$\mathbf{f}_\Theta(\mathbf{x}, \mathbf{A}) = [f_{\Theta_1}(\mathbf{x} \odot \mathbf{a}_{\cdot,1}), \dots, f_{\Theta_n}(\mathbf{x} \odot \mathbf{a}_{\cdot,n})]^T. \quad (3)$$

Here $\mathbf{a}_{\cdot,j}$ is the column vector of input causal adjacency matrix \mathbf{A} ; $f_{\phi_j} : \mathcal{X}_j \rightarrow \mathcal{Y}_j$, with $\mathcal{X}_j \subset \mathbb{R}^n$ and $\mathcal{Y}_j \subset \mathbb{R}$; the operator \odot denotes the Hadamard product.

Here function $f_{\phi_j}(\cdot)$ represents the neural network function used to approximate $f_j(\cdot)$ in Equation (1). The input to CDNN can also be \mathbf{X} with time dimension instead of \mathbf{x} , then \odot is defined as $f_{\phi_j}(\mathbf{X} \odot \mathbf{a}_{\cdot,j}) \triangleq f_{\phi_j}(\{\mathbf{x}_1 \cdot a_{1j}, \dots, \mathbf{x}_N \cdot a_{Nj}\})$. Under this definition, Cheng et al. (2023) proved that when approximating f_j with f_{ϕ_j} (along with other assumptions), the discovered causal adjacency matrix will converge to the true Granger causal matrix. Although being a CDNN, cMLP / cLSTM consists of N separate networks and is highly redundant, because the shared dynamics among different time-series are modeled N times. This redundancy not only slows down the learning process but also degrades causal discovery accuracy. Therefore, the model does not scale well to high-dimension time-series. In the following section, we introduce two techniques to alleviate the scalability issue.

CUTS+

In this work, we implement the causal graph as Causal Probability Graphs (CPGs) \mathbf{M} in which the element m_{ij} represents the probability of time-series i Granger causing j , i.e., $m_{ij} = P(x_i \rightarrow x_j)$. If \tilde{m}_{ij} in the discovered graph $\tilde{\mathbf{M}}$ is penalized to zero (or below some certain threshold), we can deduce that time-series i does not Granger cause j .

Similar to CUTS (Cheng et al. 2023), we also adapt a two-stage training strategy, and iteratively perform the **Causal**

Discovery Stage and **Prediction Stage**—the former builds a causal probability matrix with available time-series under sparse penalty, while the latter one fits the complex distribution of high-dimensional time-series and fills the missing entries. However, both stages are of totally new designs to overcome the difficulties when encountering high-dimensional time-series, as illustrated in Figure 1. Specifically, we propose to use the coarse-to-fine discovery (C2FD) technique in the Causal Discovery Stage and message-passing graph neural network (MPGNN) in the Prediction Stage, which are detailed in the following subsections.

Coarse-to-fine Causal Discovery

To address the problem of **large adjacency matrix** discussed before, we propose Coarse-to-Fine causal Discovery (C2FD). Specifically, we split the time-series into several groups, i.e., time-series group $\mathbf{X}_{\mathcal{G}_k} = \{\mathbf{x}_i\}_{i \in \mathcal{G}_k}$ where \mathcal{G}_k is the set of the indices within the k th group, and $k \in [1, N_g]$ with N_g being the group number. Each time-series is and can only be allocated to one group, i.e., $\forall k \neq l \in [1, N_g], \mathcal{G}_k \cap \mathcal{G}_l = \emptyset$. The grouping is implemented with matrix decomposition of $\tilde{\mathbf{M}}$:

$$\tilde{\mathbf{M}} = \mathbf{G}^T \mathbf{Q} \quad (4)$$

where $\mathbf{G} \in \mathbb{R}^{N_g \times N}$ is composed of entries $g_{ki} = \begin{cases} 0, & \text{if } i \notin \mathcal{G}_k \\ 1, & \text{if } i \in \mathcal{G}_k \end{cases}$. Since each time-series is and can only be allocated to one group, the sum of each column vector of \mathbf{G} is 1, i.e. $\forall i \in [1, N], \sum_{k=1}^{N_g} g_{ki} = 1$. We define the Granger causality from group $\mathbf{X}_{\mathcal{G}_k}$ as follows

Definition 2 Group $\mathbf{X}_{\mathcal{G}_k}$ is Granger non-causal of \mathbf{x}_j if there exists $\mathbf{X}'_{\mathcal{G}_k} \neq \mathbf{X}_{\mathcal{G}_k}$,

$$f_j(\{\mathbf{X}'_{\mathcal{G}_k}, \mathbf{X} \setminus \mathbf{X}_{\mathcal{G}_k}\}) = f_j(\{\mathbf{X}_{\mathcal{G}_k}, \mathbf{X} \setminus \mathbf{X}_{\mathcal{G}_k}\}) \quad (5)$$

i.e., group $\mathbf{x}_{\mathcal{G}_k}$ influence the prediction of $x_{j,t}$. Here we define $\mathbf{X} \setminus \mathbf{X}_{\mathcal{G}_k} \triangleq \{\mathbf{x}_i\}_{i \notin \mathcal{G}_k}$.

Then $\mathbf{Q} \in \mathbb{R}^{N_g \times N}$ is the Group Causal Probability Graph (GCPG) with $q_{ij} = P(\mathbf{X}_{\mathcal{G}_i} \rightarrow \mathbf{x}_j)$.

Initial Allocation. Before training, we initiate \mathbf{G} with a relatively small N_g and consequently obtain a ‘‘coarse’’ grouping. Specifically, the time series are allocated into a group following

$$|\mathcal{G}_i| = \begin{cases} \lfloor N/N_g \rfloor, & \text{if } i \in [1, N_g - 1] \\ \lfloor N/N_g \rfloor \cdot (N_g - 1), & \text{if } i = N_g. \end{cases} \quad (6)$$

Group Splitting. During training, we periodically split each group into two groups, and then N_g is doubled every 20 epochs until every group contains only one time-series. Correspondingly, when doubling group numbers, GCPG element q_{ij} is allocated to 2 elements $q_{i_1,j}$ and $q_{i_2,j}$ in the new GCPG, as initial guesses. Here we assume a group Granger cause \mathbf{x}_j if at least one sub-group Granger cause \mathbf{x}_j , then $q_{ij} = P(\mathbf{X}_{\mathcal{G}_i} \rightarrow \mathbf{x}_j) = 1 - P(\mathbf{X}_{\mathcal{G}_{i_1}} \not\rightarrow \mathbf{x}_j)P(\mathbf{X}_{\mathcal{G}_{i_2}} \not\rightarrow \mathbf{x}_j)$, where $\not\rightarrow$ denotes not Granger cause. As initial guesses we assume $P(\mathbf{X}_{\mathcal{G}_{i_1}} \rightarrow \mathbf{x}_j) = P(\mathbf{X}_{\mathcal{G}_{i_2}} \rightarrow \mathbf{x}_j)$, then $q_{i_1,j}$ and $q_{i_2,j}$ are calculated as

$$q_{i_1,j} = q_{i_2,j} = 1 - \sqrt{1 - q_{ij}}. \quad (7)$$

Convergence of C2FD. We prove the convergence of C2FD with CDNN as predictor, with a similar manner to (Cheng et al. 2023). Due to space limit, we place the detailed assumptions, theorem, and proof in Section A of the supplementary material.

The idea of coarse-to-fine is quite common in the field of machine learning (Fleuret and Geman 2001; Sarlin et al. 2019). However, to our best knowledge, we are the first to introduce the idea into neural-network-based Granger causality. Actually, the advantage of introducing C2FD is two-fold. Firstly, the parameter number to learn is greatly decreased in the initial stages. In the initial stages when $N_g \ll N$, only $N \cdot N_g$ instead of N^2 parameters are required to be optimized. Secondly, the learning results with smaller N_g serve as initial guess for learning with larger N_g . When $|\mathcal{G}_k| > 1$, GCPG element $q_{k,j}$ increases towards 1 if at least one member Granger cause time-series j . Then the whole group is used to perform data prediction with higher accuracy. After doubling N_g , the optimizer further locates the sub-group that actually Granger causes j . The empirical advantage of C2FD is validated in experiments section.

Message-passing-based Graph Neural Network

To satisfy the definition of causally disentangled neural network (CDNN) while preventing using highly redundant cMLP / cLSTM, we leverage the Message-Passing Neural Network (MPNN (Gilmer et al. 2017)) for data prediction encoder. To learn the dynamics of the high-dimensional time-series, we alter the gated recurrent units (GRUs, (Cho et al. 2014)) by adding message-passing layers. Firstly, we formulate single-layer MPNN as

$$\text{MPNN}_\nu(\mathbf{z}; \mathbf{s}) = \text{MLP}_\nu(\mathbf{z} \odot \mathbf{s}) = \mathbf{z}' \quad (8)$$

where \mathbf{h}' is the output of MPNN in the last layer, $\text{MLP}_1(\cdot)$, $\text{MLP}_2(\cdot)$ is multi-layer perceptrons (MLPs), \odot denotes the Hadamard product, and $\mathbf{s} \in \{0, 1\}^N$ is the binary causal vector, i.e., a column in the sampled Binary Causal Graph (BCG, described in Section) where $s_i = 1$ denotes z_i Granger cause the prediction. Similar to (Cini, Marisca, and Alippi 2022), we add MPNN to GRU units, which serves as a layer in MPGNN:

$$\mathbf{r}_t^j = \sigma(\text{MPNN}_{\nu_r^j}(\mathbf{x}_{:,t}; \mathbf{s}_{:,j})) \quad (9)$$

$$\mathbf{u}_t^j = \sigma(\text{MPNN}_{\nu_u^j}(\mathbf{x}_{:,t}; \mathbf{s}_{:,j})) \quad (10)$$

$$\mathbf{c}_t^j = \tanh(\text{MPNN}_{\nu_c^j}(\mathbf{x}_{:,t}; \mathbf{s}_{:,j})) \quad (11)$$

$$\mathbf{h}_t^j = \mathbf{u}_t^j \odot \mathbf{h}_{t-1}^j + (1 - \mathbf{u}_t^j) \odot \mathbf{c}_t^j, \quad (12)$$

with $\sigma(\cdot)$ being the sigmoid function. Different from standard GRU units, each gate is computed using only the input vector, which decreases parameter numbers. In the following we represent l MPGNN layers with $\text{MPGNN}_\nu(\mathbf{x}_{:,t}, \mathbf{h}_0^j; \mathbf{s}_{:,j})$, where $\nu = \{\nu_r^j, \nu_u^j, \nu_c^j, \dots, \nu_r^j, \nu_u^j, \nu_c^j\}$ (parameters of MPNNs in all layers). Note that we share ν for each j , which is the key design contributing to high scalability.

Scalability of MPGNN Encoder. The number of parameters that need to be optimized in the MPGNN encoder can be calculated as $l(|\nu^r| + |\nu^u| + |\nu^c|)$, where

l is the number of MPGNN layers. Comparing CUTS+ with component-wise GRU, whose parameter number is $Nl(|\nu^r| + |\nu^u| + |\nu^c|)$ (or cMLP / cLSTM (Tank et al. 2022) which is also $O(Nl)$), MPGNN achieves high scalability by significantly reducing the number of optimization parameters in the encoder. Moreover, since the component-wise network-based prediction model is usually overparameterized and thus prone to overfitting (Khanna and Tan 2020), our design also helps to mitigate overfitting.

Decoder. After encoding with MPGNN, the prediction result $\hat{x}_{j,t}$ is retrieved with a two-part decoder, i.e.,

$$\hat{x}_{j,t} = \text{Linear}_{\psi_j^2} \left(\text{MLP}_{\psi_1} \left(\mathbf{h}_{t-1}^j \right) \right) \quad (13)$$

where $\text{Linear}_{\psi_j^2}(\cdot)$ denotes a single linear layer with unshared weights. To capture the heterogeneity among time-series while removing structural redundancy as much as possible, here we share the weights of the first MLP part (ψ) and do not share the weight of the second single-layered part (distinct ψ_j for each target time-series j).

Overall Architecture

Bernoulli Sampling of CPG. Our CUTS+ represents causal relationships with CPG $\tilde{\mathbf{M}}$. To ensure elements of $\tilde{\mathbf{M}}$ are within range $[0, 1]$, we set $\mathbf{Q} = \sigma(\Theta)$ where Θ is the parameter to learn. During *Causal Discovery Stage* Θ is optimized using Gumbel-Softmax estimator (Jang, Gu, and Poole 2016), i.e.,

$$s_{ij} = \frac{e^{(\log(m_{ij})+g)/\tau}}{e^{(\log(m_{ij})+g)/\tau} + e^{(\log(1-m_{ij})+g)/\tau}} \quad (14)$$

Where $g = -\log(-\log(u))$, $u \sim \text{Uniform}(0, 1)$. We use a large τ in the initial stages then decrease to a small value. This estimator has a relatively low variance, mimic Bernoulli distribution when τ is small, and more importantly, enables continuous optimization of Θ .

During *Prediction Stage*, CPG $\tilde{\mathbf{M}}$ is sampled to binary causal graph (BCG) \mathbf{S} where $s_{ij} \sim \text{Ber}(m_{ij})$. Finally BCG columns $\mathbf{s}_{:,j}$ is used as adjacency matrix in MPNNs.

Loss Functions. CUTS+ iterates between *Causal Discovery Stage* and *Prediction Stage*. During the former stage, only the CPG $\tilde{\mathbf{M}} = \sigma(\Theta)$ will be optimized, so the optimization problem is

$$\max_{\Theta} \mathcal{L}_{\text{graph}} = \max_{\Theta} \frac{\sum_{j=1}^N \sum_{t=1}^T (\hat{x}_{j,t} - x_{j,t})^2 \cdot o_{j,t}}{\sum_{j=1}^N \sum_{t=1}^T o_{j,t}} + \lambda \|\sigma(\Theta)\|_1. \quad (15)$$

In the latter stage, we only optimize the network parameters:

$$\max_{\Phi} \mathcal{L}_{\text{data}} = \max_{\Phi} \frac{\sum_{j=1}^N \sum_{t=1}^T (\hat{x}_{j,t} - x_{j,t})^2 \cdot o_{j,t}}{\sum_{j=1}^N \sum_{t=1}^T o_{j,t}}. \quad (16)$$

where $\Phi = \{\nu, \psi_1, \{\psi_j^j\}_{j=1}^N\}$ is all network parameters in MPGNN encoder and decoder.

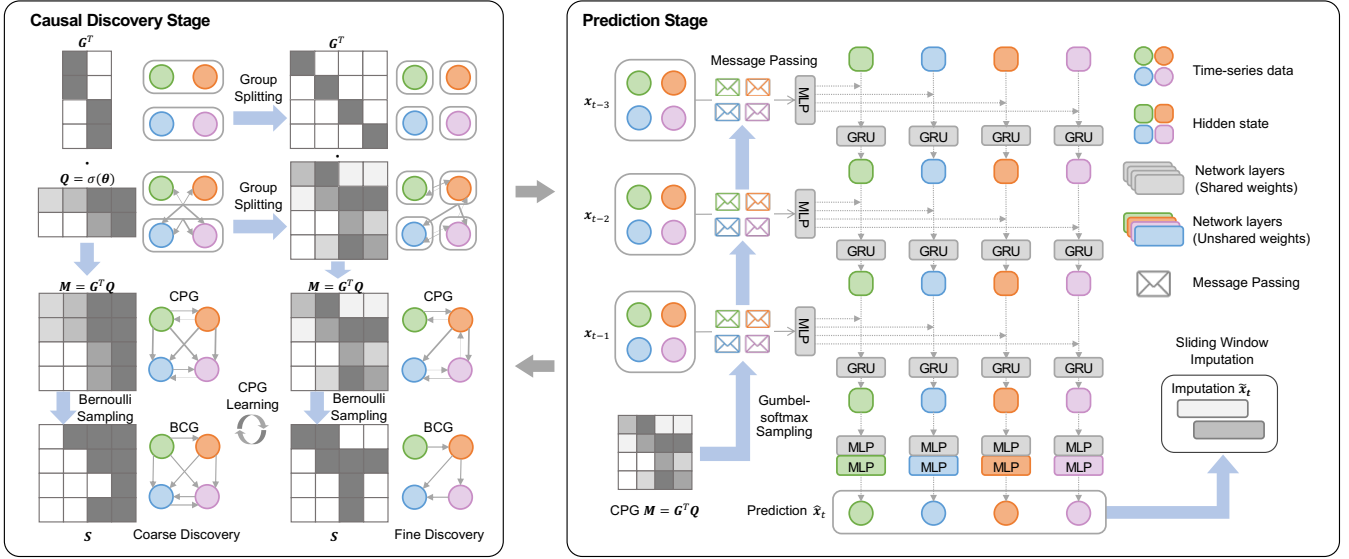


Figure 1: The architecture of CUTS+ with two alternating stages, both boosted for high-dimensional causal discovery. The **Causal Discovery Stage** is equipped with Coarse-to-fine Causal Discovery (C2FD) while the **Prediction Stage** is with Message-passing-based Graph Neural Network (MPGNN).

Satisfaction of CDNN. CDNN in Definition 1 is satisfied when a column of the matrix \mathbf{A} only affects the corresponding component of the prediction $\mathbf{f}_\Phi(x, \mathbf{A})$. If we combine the prediction module $\text{MPGNN}_\nu(\tilde{\mathbf{X}}, \mathbf{h}_0^j; \mathbf{s}_{:,j})$ with $\text{Linear}_{\psi_j^2}(\text{MLP}_{\psi^1}(\cdot))$, we get

$$\hat{x}_{:,t} = \mathbf{f}_\Phi(\mathbf{X}, \mathbf{S}) = \left[\dots, \text{Linear}_{\psi_j^2} \left(\text{MLP}_{\psi^1} \left(\text{MPGNN}_\nu \left(\tilde{\mathbf{X}}, \mathbf{h}_0^j; \mathbf{s}_{:,j} \right) \right) \right), \dots \right]^T \quad (17)$$

where \mathbf{h}_0^j is the initial value of GRU hidden states and irrelevant to \mathbf{x} . Therefore, our CUTS is a CDNN, and according to Theorem 1 in supplementary Section A, the correct causal graph can be recovered.

Handling Irregular Time-series with Imputation. In this work, we handle irregular time-series by performing concurrent data imputation during **Prediction Stage**. Our data imputation is performed with sliding windows, where the missing entries in one time window are filled with the prediction $\hat{x}_{j,t}$ from the last windows. Due to page limits, we place the details for sliding window imputation in supplementary Section C.3.

Experiments

In this section, we quantitatively evaluate the proposed CUTS+ and comprehensively compare it with state-of-the-art methods to validate our design.

Baseline Algorithms. To demonstrate its advantageous performance, we compared CUTS+ with 7 baseline algorithms: (i) Neural Granger Causality (NGC, (Tank et al. 2022)), which utilizes cMLP and cLSTM to infer Granger causal relationships; (ii) economy-SRU (eSRU, (Khanna

and Tan 2020)), a variant of SRU that is less prone to over-fitting when inferring Granger causality; (iii) PCMCI (Runge et al. 2019), a non-Granger-causality-based method that uses conditional independence tests; (iv) Latent Convergent Cross Mapping (LCCM, (Brouwer et al. 2021)), a CCM-based approach that also tackles the irregular time-series problem; (v) Neural Graphical Model (NGM, (Bellot, Branson, and van der Schaar 2022)), which uses Neural Ordinary Differential Equations (Neural-ODE) to handle irregular time-series data; (vi) Scalable Causal Graph Learning (SCGL, (Xu, Huang, and Yoo 2019)) that address scalable causal discovery problem with low-rank assumption; and (vii) CUTS (Cheng et al. 2023). We evaluated the performance in terms of the area under the ROC curve (AUROC) criterion. For a fair comparison, we search the best hyperparameters for the baseline algorithms on the validation dataset, and test performances on testing sets for 5 random seeds per experiment. For the baseline algorithms that could not handle irregular time-series data, i.e., NGC, PCMCI, SCGL, and eSRU, we imputed the irregular time-series using two algorithms: Zero-order Holder (ZOH, filling with the nearest historical sample, does not introduce future samples), and state-of-the-art imputation algorithm TimesNet (Wu et al. 2023).

Ablation Study Settings. Our main technical contributions are introducing C2FD and MPGNN into causal discovery. To quantitatively validate these two techniques, we add C2FD into the original CUTS (Cheng et al. 2023) to get “CUTS with C2FD”. Consequently, we can measure C2FD’s performance gain by comparing “CUTS” with “CUTS with C2FD” and verify MPGNN by comparing “CUTS with C2FD” with “CUTS+”.

Datasets. We assess the performance of the causal

Method	Imputation	VAR with RM ($N = 128$)		VAR with RBM ($N = 128$)		VAR ($N = 128$) No missing
		$p = 0.3$	$p = 0.6$	$p_{\text{blk}} = 0.15\%$	$p_{\text{blk}} = 0.3\%$	
NGC	ZOH	0.8234 \pm 0.0082	0.7419 \pm 0.0056	0.8638 \pm 0.0165	0.8357 \pm 0.0161	0.9168 \pm 0.0087
	TimesNet	0.7900 \pm 0.0111	0.6560 \pm 0.0112	0.8519 \pm 0.0056	0.8292 \pm 0.0083	
eSRU	ZOH	0.6627 \pm 0.0071	0.6711 \pm 0.0097	0.6606 \pm 0.0152	0.6457 \pm 0.0060	0.6860 \pm 0.0144
	TimesNet	0.6175 \pm 0.0149	0.5671 \pm 0.0156	0.6643 \pm 0.0097	0.6488 \pm 0.0096	
SCGL	ZOH	0.6627 \pm 0.0071	0.6711 \pm 0.0097	0.6606 \pm 0.0152	0.6457 \pm 0.0060	0.6519 \pm 0.0078
	TimesNet	0.6536 \pm 0.0180	0.6542 \pm 0.0048	0.6558 \pm 0.0118	0.6631 \pm 0.0138	
	NGM	0.5815 \pm 0.0494	0.5016 \pm 0.0010	0.5918 \pm 0.0700	0.5003 \pm 0.0004	
CUTS		0.9434 \pm 0.0123	0.8814 \pm 0.0151	0.9579 \pm 0.0085	0.9505 \pm 0.0091	0.9626 \pm 0.0057
CUTS with C2FD		0.9594 \pm 0.0094	0.8752 \pm 0.0183	0.9742 \pm 0.0061	0.9651 \pm 0.0072	0.9875 \pm 0.0024
CUTS+		0.9907 \pm 0.0008	0.9569 \pm 0.0051	0.9939 \pm 0.0018	0.9912 \pm 0.0025	0.9972 \pm 0.0005

Method	Imputation	Lorenz-96 with RM ($N = 256$)		Lorenz-96 with RBM ($N = 256$)		Lorenz-96 ($N = 256$) No missing
		$p = 0.3$	$p = 0.6$	$p_{\text{blk}} = 0.15\%$	$p_{\text{blk}} = 0.3\%$	
NGC	ZOH	0.9755 \pm 0.0092	0.8469 \pm 0.0331	0.9893 \pm 0.0022	0.9760 \pm 0.0042	0.9937 \pm 0.0014
	TimesNet	0.9415 \pm 0.0183	0.5000 \pm 0.0000	0.9685 \pm 0.0070	0.7965 \pm 0.0442	
eSRU	ZOH	0.9735 \pm 0.0019	0.8972 \pm 0.0046	0.9821 \pm 0.0019	0.9728 \pm 0.0016	0.9908 \pm 0.0005
	TimesNet	0.9618 \pm 0.0044	0.8742 \pm 0.0047	0.9794 \pm 0.0042	0.9762 \pm 0.0033	
SCGL	ZOH	0.6191 \pm 0.0090	0.5182 \pm 0.0109	0.6308 \pm 0.0061	0.6195 \pm 0.0069	0.6620 \pm 0.0083
	TimesNet	0.6210 \pm 0.0032	0.5280 \pm 0.0060	0.6312 \pm 0.0072	0.6054 \pm 0.0034	
	NGM	0.9620 \pm 0.0072	0.6125 \pm 0.0372	0.9831 \pm 0.0031	0.9866 \pm 0.0006	
CUTS		0.9360 \pm 0.0043	0.8668 \pm 0.0043	0.9430 \pm 0.0030	0.9330 \pm 0.0053	0.9571 \pm 0.0027
CUTS with C2FD		0.9790 \pm 0.0016	0.9069 \pm 0.0036	0.9874 \pm 0.0009	0.9834 \pm 0.0015	0.9992 \pm 0.0000
CUTS+		0.9984 \pm 0.0002	0.9916 \pm 0.0016	0.9989 \pm 0.0003	0.9985 \pm 0.0002	0.9992 \pm 0.0002

Table 2: Performance comparison of CUTS+ with NGC, eSRU, NGM, SCGL, and CUTS combined with ZOH and TimesNet for imputation. We do not perform comparison experiments with PCMCi and LCCM, because with a large N and T , the running times for these two methods are extremely long. Comparisons to them are performed on Dream-3 datasets (Table 3).

discovery approach CUTS+ on three types of datasets: simulated data, quasi-realistic data (i.e., synthesized under physically meaningful causality), and real data. Simulated datasets include linear Vector Autoregressive (VAR) and nonlinear Lorenz-96 models (Karimi and Paul 2010), quasi-realistic datasets are from Dream-3 (Prill et al. 2010), while real datasets include Air Quality datasets from 163 monitor stations across 20 Chinese cities. Irregular observations are generated via Random Missing (RM) and Random Block Missing (RBM). For statistical evaluation of causal discovery algorithms, we average over results on simulations from 5 different random seeds. In the following experiments, we also show the standard derivations.

Results on Simulated Datasets

VAR. VAR datasets are simulated with the linear equation $\mathbf{x}_{:,t} = \sum_{\tau=1}^{\tau_{max}} \mathbf{A} \mathbf{x}_{:,t-\tau} + \mathbf{e}_{:,t}$, where the matrix \mathbf{A} is the causal coefficients and $\mathbf{e}_{:,t} \sim \mathcal{N}(\mathbf{0}, \sigma \mathbf{I})$. Time-series i Granger cause time-series j if $a_{ij} > 0$. The objective of causal discovery is to find the non-zero elements in a causal graph \mathbf{A} with \mathbf{M} . We set $\tau_{max} = 3$ and time-series length $L = 1000$ in this experiment. One can observe in Table 2 that CUTS+ beats all other algorithms with a clear margin. Moreover, we perform comparison experiments on VAR datasets with different graph densities in supplementary Section B.1.

Lorenz-96. Lorenz-96 datasets are simulated accord-

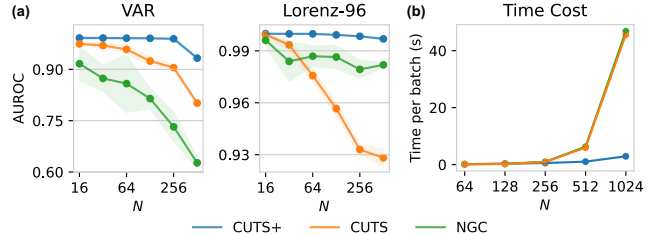


Figure 2: Experiments on scalability of the models. (a) Comparison of scalability with CUTS and NGC in terms of AUROC (RM with $p = 0.3$). (b) Time cost of CUTS+ comparing with NGC and CUTS+, on $N = 64, 128, 256, 512, 1024$.

ing to $\frac{dx_{i,t}}{dt} = -x_{i-1,t}(x_{i-2,t} - x_{i+1,t}) - x_{i,t} + F$, where we set $F = 10, L = 1000$. In this model each time-series \mathbf{x}_i is affected by historical values of four time-series $\mathbf{x}_{i-2}, \mathbf{x}_{i-1}, \mathbf{x}_i, \mathbf{x}_{i+1}$, and each row in the true causal graph \mathbf{A} has four non-zero elements. Table 2 shows that CUTS+ is advantageous over other algorithms.

Ablation Study. By comparing ‘‘CUTS’’, ‘‘CUTS with C2FD’’, and ‘‘CUTS+’’, we see that both C2FD and MPGNN contribute to the performance gain. C2FD is relatively more helpful on Lorenz-96, and MPGNN helps more on VAR.

Scalability. The VAR and Lorenz-96 datasets support setting N . To demonstrate CUTS+’s scalability to high dimensional data, we compare CUTS+ with the two best-

Methods	Dream-3 ($N = 100$, No missing)
PCMCI	0.5517 ± 0.0261
NGC	0.5579 ± 0.0313
eSRU	0.5587 ± 0.0335
SCGL	0.5273 ± 0.0276
LCCM	0.5046 ± 0.0318
NGM	0.5477 ± 0.0252
CUTS	0.5915 ± 0.0344
CUTS with C2FD	0.6123 ± 0.0497
CUTS+	0.6374 ± 0.0740

Table 3: Performance comparison of CUTS+ with PCMCI, NGC, eSRU, NGM, SCGL, LCCM and CUTS on Dream-3 datasets without missing values.

performing algorithms, i.e., CUTS and NGC (combining ZOH). We set the same average numbers for causal parents in VAR when N changes. Shown in Figure 2(a), by increasing the time series number N of VAR and Lorenz-96 datasets, we observe that AUROC of CUTS and NGC degrades significantly when N increases on both datasets. On the contrary, CUTS+ beats both algorithms with a clear margin, and the advantages are especially prominent with a large N . The performance for CUTS+ only degrades clearly when $N = 512$ on VAR datasets. More scalability experiments with multiple types of irregular sampling or no missing values are shown in supplementary Section B.2.

Our advantages over other approaches also exists in terms of computational complexity. Shown in Figure 2(b) are the time costs for each forward+backward propagation. We compare the network in our CUTS+ with cMLP and cLSTM in NGC and CUTS. The results show that the computational costs are greatly reduced when comparing to cMLP and cLSTM, especially when $N > 256$.

Results on Quasi-Realistic Datasets

Dream-3. Dream-3 (Prill et al. 2010) is a gene expression and regulation dataset widely used as causal discovery benchmarks (Khanna and Tan 2020; Tank et al. 2022). This dataset contains 5 models, each representing measurements of 100 gene expression levels. The length of each measured trajectory is $T = 21$, which is too short to perform RM or RBM, so we only compare with baselines for time-series without data missing on Dream-3. The results are listed in Table 3, which shows that our CUTS+ performs better than the others, proving that our approach can also handle data without missing entries.

As for the ablation study, we observe that MPGNN and C2FD both contribute clearly, each with performance gain of more than 0.02 in terms of AUROC.

Results on Real Datasets

Air Quality (AQI). We test our CUTS+ on AQI, a real high-dimensional dataset with $N = 163, T = 8760$ (detailed description of this dataset is in supplementary Section C.2). We do not have access to the ground-truth causal graph because of the extremely complex atmosphere physics, so

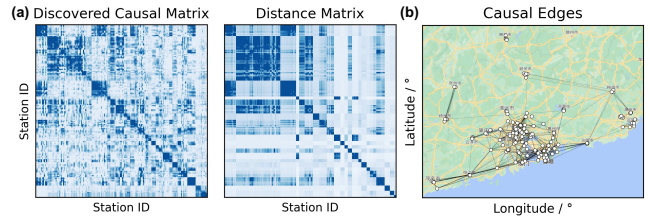


Figure 3: Causal discovery result on AQI dataset. (a) Causal discovery results on AQI dataset compared with the distance matrix (which might indicate the true causal graph) (b) Causal discovery results plot overlaid on the map.

quantitative performance evaluation and comparisons with baselines may be less persuasive (shown in supplementary Section B.3). However, we have a prior that the real causal relationships are very closely related to the geometrical distances. Therefore, to verify the causal discovery results of CUTS+, we compare the discovered CPG $\tilde{\mathbf{M}}$ (Figure 3(a) left) with the distance matrix \mathbf{D} (where its element $d_{ij} \propto 1/\text{dist}(i, j)$, Figure 3(a) right). It can be observed that the discovered causal matrix does mimic the distance matrix. We also plotted the CPG edges with $P(i \rightarrow j) > 0.5$ on the map (Figure 3(b)), which shows that most of the causal edges discovered connect the stations not far apart. This indirectly demonstrates the effectiveness of CUTS+ on real high-dimensional data.

Additional Information

The assumptions, theorems and proof for the convergence of CPG in our CUTS+ are provided in the supplementary Section A. In Section B, we perform other supplementary experiments, including experiments on graph density, scalability, and quantitative comparison on AQI dataset. We provide implementation details for CUTS in Section C, including network structure, hyper-parameters for each experiment, configuration for RM and RBM, and detailed settings for baseline algorithms. Additionally, we list the broader impacts and limitations in Sections D and E.

Conclusions

We propose CUTS+, a Granger-causality-based causal discovery approach, to handle high-dimensional time-series with irregular sampling. We largely improve the scalability with respect to the data dimension by (a) introducing Coarse-to-fine Discovery (C2FD) to resolve the large CPG problem and (b) designing a Message-passing-based Graph Neural Network (MPGNN) to address the redundant network parameters problem. Comparing to previous approaches, CUTS+ largely increases AUROC and decrease time cost especially when confronted with high dimensional time series. Our future works include: (i) High-dimensional causal discovery with latent confounder or instantaneous effect. (ii) Explaining neural network with causal models. Our code is available at <https://github.com/jarrycyx/unnc>.

Acknowledgments

This work is jointly funded by Ministry of Science and Technology of China (Grant No. 2020AAA0108202), National Natural Science Foundation of China (Grant No. 61931012 and 62088102), Beijing Natural Science Foundation (Grant No. Z200021), and Project of Medical Engineering Laboratory of Chinese PLA General Hospital (Grant No. 2022SYSZZKY21).

References

- Bellot, A.; Branson, K.; and van der Schaar, M. 2022. Neural Graphical Modelling in Continuous-Time: Consistency Guarantees and Algorithms. In *International Conference on Learning Representations*.
- Benkó, Z.; Zlatniczki, Á.; Stippinger, M.; Fabó, D.; Sólyom, A.; Erőss, L.; Telcs, A.; and Somogyvári, Z. 2020. Complete Inference of Causal Relations between Dynamical Systems. arxiv:1808.10806.
- Brouwer, E. D.; Arany, A.; Simm, J.; and Moreau, Y. 2021. Latent Convergent Cross Mapping. In *International Conference on Learning Representations*.
- Cheng, Y.; Yang, R.; Xiao, T.; Li, Z.; Suo, J.; He, K.; and Dai, Q. 2023. CUTS: Neural Causal Discovery from Irregular Time-Series Data. In *The Eleventh International Conference on Learning Representations*.
- Cho, K.; van Merriënboer, B.; Gulcehre, C.; Bahdanau, D.; Bougares, F.; Schwenk, H.; and Bengio, Y. 2014. Learning Phrase Representations Using RNN Encoder-Decoder for Statistical Machine Translation. arxiv:1406.1078.
- Cini, A.; Marisca, I.; and Alippi, C. 2022. Filling the G_{ap}s: Multivariate Time Series Imputation by Graph Neural Networks. In *International Conference on Learning Representations*.
- Cundy, C.; Grover, A.; and Ermon, S. 2021. BCD Nets: Scalable Variational Approaches for Bayesian Causal Discovery. In *Advances in Neural Information Processing Systems*, volume 34, 7095–7110. Curran Associates, Inc.
- Fleuret, F.; and Geman, D. 2001. Coarse-to-Fine Face Detection. *International Journal of Computer Vision*, 41(1): 85–107.
- Geffner, T.; Antoran, J.; Foster, A.; Gong, W.; Ma, C.; Kici-man, E.; Sharma, A.; Lamb, A.; Kukla, M.; Pawlowski, N.; Allamanis, M.; and Zhang, C. 2022. Deep End-to-end Causal Inference. arxiv:2202.02195.
- Gerhardus, A.; and Runge, J. 2020. High-Recall Causal Discovery for Autocorrelated Time Series with Latent Confounders. In *Advances in Neural Information Processing Systems*, volume 33, 12615–12625. Curran Associates, Inc.
- Gilmer, J.; Schoenholz, S. S.; Riley, P. F.; Vinyals, O.; and Dahl, G. E. 2017. Neural Message Passing for Quantum Chemistry. In *Proceedings of the 34th International Conference on Machine Learning*, 1263–1272. PMLR.
- Granger, C. W. J. 1969. Investigating Causal Relations by Econometric Models and Cross-Spectral Methods. *Econometrica*, 37(3): 424–438.
- Hong, Y.; Liu, Z.; and Mai, G. 2017. An Efficient Algorithm for Large-Scale Causal Discovery. *Soft Computing*, 21(24): 7381–7391.
- Hoyer, P.; Janzing, D.; Mooij, J. M.; Peters, J.; and Schölkopf, B. 2008. Nonlinear Causal Discovery with Additive Noise Models. In *Advances in Neural Information Processing Systems*, volume 21. Curran Associates, Inc.
- Jang, E.; Gu, S.; and Poole, B. 2016. Categorical Reparameterization with Gumbel-Softmax.
- Karimi, A.; and Paul, M. R. 2010. Extensive Chaos in the Lorenz-96 Model. *Chaos: An Interdisciplinary Journal of Nonlinear Science*, 20(4): 043105.
- Khanna, S.; and Tan, V. Y. F. 2020. Economy Statistical Recurrent Units for Inferring Nonlinear Granger Causality. In *International Conference on Learning Representations*.
- Lopez, R.; Huetter, J.-C.; Pritchard, J.; and Regev, A. 2022. Large-Scale Differentiable Causal Discovery of Factor Graphs. *Advances in Neural Information Processing Systems*, 35: 19290–19303.
- Löwe, S.; Madras, D.; Zemel, R.; and Welling, M. 2022. Amortized Causal Discovery: Learning to Infer Causal Graphs from Time-Series Data. In *Proceedings of the First Conference on Causal Learning and Reasoning*, 509–525. PMLR.
- Morales-Alvarez, P.; Gong, W.; Lamb, A.; Woodhead, S.; Peyton Jones, S.; Pawlowski, N.; Allamanis, M.; and Zhang, C. 2022. Simultaneous Missing Value Imputation and Structure Learning with Groups. *Advances in Neural Information Processing Systems*, 35: 20011–20024.
- Pamfil, R.; Sriwattanaworachai, N.; Desai, S.; Pilgerstorfer, P.; Georgatzis, K.; Beaumont, P.; and Aragam, B. 2020. DYNOTEARS: Structure Learning from Time-Series Data. In *Proceedings of the Twenty Third International Conference on Artificial Intelligence and Statistics*, 1595–1605. PMLR.
- Peters, J.; Janzing, D.; and Schölkopf, B. 2017. *Elements of Causal Inference: Foundations and Learning Algorithms*. The MIT Press. ISBN 978-0-262-03731-0 978-0-262-34429-6.
- Prill, R. J.; Marbach, D.; Saez-Rodriguez, J.; Sorger, P. K.; Alexopoulos, L. G.; Xue, X.; Clarke, N. D.; Altan-Bonnet, G.; and Stolovitzky, G. 2010. Towards a Rigorous Assessment of Systems Biology Models: The DREAM3 Challenges. *PLOS ONE*, 5(2): e9202.
- Runge, J. 2020. Discovering Contemporaneous and Lagged Causal Relations in Autocorrelated Nonlinear Time Series Datasets. In *Proceedings of the 36th Conference on Uncertainty in Artificial Intelligence (UAI)*, 1388–1397. PMLR.
- Runge, J.; Nowack, P.; Kretschmer, M.; Flaxman, S.; and Sejdinovic, D. 2019. Detecting and Quantifying Causal Associations in Large Nonlinear Time Series Datasets. *Science Advances*, 5(11): eaau4996.
- Sarlin, P.-E.; Cadena, C.; Siegwart, R.; and Dymczyk, M. 2019. From Coarse to Fine: Robust Hierarchical Localization at Large Scale. In *Proceedings of the IEEE/CVF Conference on Computer Vision and Pattern Recognition*, 12716–12725.

- Shimizu, S.; Hoyer, P. O.; Hyvä, A.; rinen; and Kerminen, A. 2006. A Linear Non-Gaussian Acyclic Model for Causal Discovery. *Journal of Machine Learning Research*, 7(72): 2003–2030.
- Spirtes, P.; and Glymour, C. 1991. An Algorithm for Fast Recovery of Sparse Causal Graphs. *Social science computer review*, 9(1): 62–72.
- Spirtes, P.; Glymour, C. N.; Scheines, R.; and Heckerman, D. 2000. *Causation, Prediction, and Search*. MIT press.
- Sugihara, G.; May, R.; Ye, H.; Hsieh, C.-h.; Deyle, E.; Fogarty, M.; and Munch, S. 2012. Detecting Causality in Complex Ecosystems. *Science*, 338(6106): 496–500.
- Tank, A.; Covert, I.; Foti, N.; Shojaie, A.; and Fox, E. B. 2022. Neural Granger Causality. *IEEE Transactions on Pattern Analysis and Machine Intelligence*, 44(8): 4267–4279.
- Vowels, M. J.; Camgoz, N. C.; and Bowden, R. 2021. D’ya like Dags? A Survey on Structure Learning and Causal Discovery. arxiv:2103.02582.
- Wu, A. P.; Singh, R.; and Berger, B. 2022. Granger Causal Inference on Dags Identifies Genomic Loci Regulating Transcription. In *International Conference on Learning Representations*.
- Wu, H.; Hu, T.; Liu, Y.; Zhou, H.; Wang, J.; and Long, M. 2023. TimesNet: Temporal 2D-Variation Modeling for General Time Series Analysis. In *The Eleventh International Conference on Learning Representations*.
- Xu, C.; Huang, H.; and Yoo, S. 2019. Scalable Causal Graph Learning through a Deep Neural Network. In *Proceedings of the 28th ACM International Conference on Information and Knowledge Management, CIKM ’19*, 1853–1862. New York, NY, USA: Association for Computing Machinery. ISBN 978-1-4503-6976-3.
- Ye, H.; Deyle, E. R.; Gilarranz, L. J.; and Sugihara, G. 2015. Distinguishing Time-Delayed Causal Interactions Using Convergent Cross Mapping. *Scientific Reports*, 5(1): 14750.
- Yi, X.; Zheng, Y.; Zhang, J.; and Li, T. 2016. ST-MVL: Filling Missing Values in Geo-Sensory Time Series Data. In *Proceedings of the 25th International Joint Conference on Artificial Intelligence*.